Geoderma 404 (2021) 115292

Contents lists available at ScienceDirect

Geoderma

journal homepage: www.elsevier.com/locate/geoderma

Soil burrow characterization by 3D image analysis: Prediction of macroinvertebrate groups from biopore size distribution parameters

Giacomo Mele [a], Gilda Buscemi [b], Laura Gargiulo [a,*], Fabio Terribile [b]

[a] Institute for Agricultural and Forest Systems in the Mediterranean (ISAFoM), Department of Biology, Agriculture and Food Sciences (DiSBA), National Research Council (CNR), P.le Enrico Fermi 1 - Loc. Porto del Granatello, 80055 Portici, NA, Italy
[b] Department of Agriculture, University of Napoli Federico II, Via Università 100, 80055 Portici, NA, Italy

ARTICLE INFO

Handling Editor: Yvan Capowiez

Keywords:
Soil fauna
X-ray tomography
Macropores
FFT
Discriminant Analysis

ABSTRACT

Although scientific literature focuses mainly on earthworms, all soil macroinvertebrates play an important role in modifying the architecture of the soil pore space and, in turn, in soil functions. Notwithstanding the fact that non-invasive technology, such as X-ray tomography, has long been used to differentiate non-biopores from biopores, it is still difficult to distinguish the specific contribution different macroinvertebrates make to the soil biopore system. Unlike the object-based image analysis approach, when applied to a soil pore system, mathematical morphology permits the user to obtain a very accurate pore size distribution consistent with the physical principle of water retention. The aim of this work was to evaluate the potential of the parameters of this kind of biopore size distribution to differentiate between the burrows of five different macroinvertebrate groups, namely Earthworms, Millipedes juliform, Centipedes, Campodeiform larvae and Elateriform larvae, inoculated into repacked soil mesocosms and incubated (14 days) in the field from where the soil animals were originally collected.

A two-fold approach was proposed in this work so as to obtain parameters by both pore size population distributions and Weibull modelling of the cumulative distributions. Then a predictive discriminant analysis was performed on selected parameters by using macroinvertebrate groups as grouping variables and a very good prediction was obtained in both cases. The most useful parameters were the skewness and FFT indices in the first case and the shape parameter α of the Weibull model along with its RMSE in the second one. In addition, topological characterization was performed on gallery-shaped biopores. Vertical deviation was the only parameter that was independent of the individual body size and showed the statistically significant lowest value for the earthworms. The experiment and analyses performed in this work to explore the connection between macroinvertebrate groups and the corresponding biopore size distributions may represent a suitable methodological approach to performing a general investigation into the relationships between soil management and its impact on the system of soil macropores.

1. Introduction

The role of soil fauna in soil functioning has been emphasized in ecological science in the concept of "physical ecosystem engineering" (Jones et al., 1994; Wright and Jones, 2006; Lavelle et al., 2016). Soil macroinvertebrates such as earthworms, ants, termites and myriapods all modify the physical architecture of their habitat, the soil pore space (e.g., Khan et al., 2018; Schon et al., 2017; Drager et al., 2016; Bowen and Hembree, 2014) through their different burrowing mechanisms (e.g., Ruiz and Or, 2018; Kime and Golovatch, 2000). Such biological activity affects soil structure dynamics on different time and length scales (e.g., Meurer et al., 2020) and induces macroscopic changes in soil physical properties. For example, soil fauna activity influences water infiltration (e.g.; Cheik et al., 2019; Schon et al., 2017) as well as the distribution and functioning of microorganisms in the soil (e.g., Medina-Sauza et al., 2019; Kuzyakov and Blagodatskaya, 2015).

Since the beginning of the 90 s, non-invasive technology such as X-ray CT has been increasingly applied as a useful tool in order to observe directly and quantify macroinvertebrate burrows in soil (e.g., Helliwell et al., 2013; Bastardie et al., 2005; Daniel et al., 1997; Joschko et al., 1993) by using 3D image analysis. Most of authors inoculated repacked soil cores with earthworms and incubated them in growth chambers (e.

* Corresponding author.
E-mail address: laura.gargiulo@cnr.it (L. Gargiulo).

https://doi.org/10.1016/j.geoderma.2021.115292
Received 10 December 2020; Received in revised form 28 May 2021; Accepted 6 June 2021

g., Baccaro et al., 2019; Capowiez et al., 2011) or alternatively collected undisturbed soil cores to study the soil biopore network that had developed in the field (e.g., Cheik et al., 2019; Pierret et al., 2003).

Many approaches to the characterization of biopore systems have been applied by means of different image analysis procedures. In many cases, after segmentation of the biopore space from imaged soil cores, topological analysis of the gallery network was conducted by means of the 3D skeletonization procedure, determining useful parameters like length, tortuosity, and vertical deviation of segments of a burrow system (e.g., Balseiro-Romero et al., 2020; Capowiez et al., 2011, 2015, 2014). In other cases, soil biopore space has been characterized in terms of its size distribution (e.g., Baccaro et al., 2019; Porre et al., 2016; Bastardie et al., 2003; Pierret et al., 2003; Capowiez et al., 2003), which is obtainable through devoted mathematical morphology procedures (e.g., Serra et al., 1982; Horgan, 1998). Actually, Pierret et al. (2002) pointed out advantages of such kind of pore size distribution for its consistency with the physical principle of water retention. Moreover, as skeletonization of irregular pores may produce noisy skeletons and causes overestimation of the biopore length (Zhang et al., 2018), pore size distribution has the advantage of being relevant in the characterization of any kind of biopore space, even when macroinvertebrate burrowing activity does not produce galleries.

Overall, understanding the specific contribution of different soil faunal groups to the biopore system by means of effective quantification approaches still remains a challenge.

In this framework, we carried out an experiment with repacked soil mesocosms inoculated with five different groups of macroinvertebrates, incubated in the same field where the soil fauna was collected. The mesocosms were imaged by means of X-ray tomography and the biopores were characterized by using mathematical morphology procedures with the aim of evaluating the potential of the pore size distribution parameters for differentiating between the burrowing activity of each macroinvertebrate group. The burrow system of the macroinvertebrate groups producing galleries was characterized, in addition, by topological parameters.

2. Materials and methods

2.1. The used soil and soil macroinvertebrates

The soil and macroinvertebrates used for the experiment were collected at the beginning of June 2015 from an experimental orchard at the base of the Mount Vesuvius (40.838050 N, 14.364308E) in Ercolano, South Italy. The soil, a Vitric Andosol according to WRB (IUSS Working Group WRB, 2014), was sampled from the first 10 cm of topsoil and the main soil properties are reported in table 1.

The collection of soil macroinvertebrates was carried out by digging 5 soil pits of 25x25 cm to a depth of 10 cm. The macroinvertebrate individuals were hand-sorted in the laboratory and kept alive in different containers, while soil was sieved to 2 mm and stored for a few days in a dark chamber at 12 °C before preparing soil mesocosms. After the identification of the sampled fauna in terms of their taxonomic rank of family (genus is reported in bracket), the taxa to be used for the experiment were chosen on the basis of their different body shapes and burrowing behaviour. In particular, we chose these five families (genus) of macroinvertebrates: Lumbricidae (Lumbricus), Julidae (Pachyiulus), Geophilidae (Geophilus), Staphylinidae (Ocypus), Elateridae (Agriotes), belonging to the following different morphotype groups: Earthworms (W), juliform Millipedes (M), Centipedes (C), Campodeiform larvae (Cl) and Elateriform larvae (El), respectively. For each group, three individuals were chosen and numbered "1, 2 and 3" from the smallest to the largest specimen, respectively. Each individual was inoculated into a different soil mesocosm.

Table 1
Main properties of the soil used in the experiment (fine fraction < 2 mm).

Sand	Silt	Clay	pH (H_2O)	OM [a]	$CaCO_3$	CEC [b]
(%)	(%)	(%)		(%)	(%)	(cmol(+)Kg^{-1})
74.9	18.1	6.1	7.45	5.9	1.87	25.2

[a] Organic matter

[b] Cation exchange capacity

Before the inoculation of the sieved soil mesocosms with soil fauna, calibrated digital photographs of the chosen macroinvertebrates were taken and their body size was measured by using the Image Pro-Premier 9.1 image analysis software (www.mediacy.com). Body diameter was measured by using a digital calliper tool at five different points along the body and the averaged value was determined. For calculation of the body volume, we assumed a cylindrical body shape for all organisms except for Centipedes, which we assumed had an elliptical body section with a 1.3 major/minor axis ratio. In the following text, the diameter of group C represents the major axis. The measured body size parameters are reported in Table 2.

2.2. Mesocosms preparation

Fifteen repacked soil cores (3 for each macroinvertebrate group) were prepared using 5 cm high PVC cylinders (7 cm for earthworms) with a diameter of 5 cm (6 cm for earthworms). The bottom of each core was sealed and they were filled with 2 mm sieved soil up to 1 cm from the top. During the filling, each core was gently shaken and one dry-wet cycle was performed in order to allow a uniform soil settlement, which corresponded to a completely unstructured soil matrix. Mesocosms were then re-wet to about 65% of the field capacity. One individual and food (dried grass) were added to the top of each core. The top of each core was closed using a 0.25 mm mesh nylon gauze in order to keep the soil animals within the mesocosm.

At the end of June, the cores were incubated within the same site from which the initial collection was made, inserting the cores into soil to a depth of 10 cm in order to put the specimens into environmental conditions as similar as possible to those they naturally experience. After two weeks, the cores were gently recovered from the field and imaged through medical X-ray tomography.

2.3. Biopore imaging

Imaging of the biopores inside the cores was performed with the TAC Discovery CT750 HD (General Electric) medical X-ray tomograph at the SDN Institute of Diagnostic and Nuclear Medicine Research in Napoli. The X-ray source was set at 120 kV and 120 mA, obtaining a stack of images each with a resolution of 200 μm/pixel and spaced at 625 μm intervals. Images (16-bits DICOM format), whose minimum and maximum gray-level values were set at −1000 and 2000 HU, respectively, were converted into 8-bit BMP images by using CTAn software (www.bruker.com). The stack of images was processed in order to reconstruct the internal structure of each soil mesocosm by using a volume representation with a cubic grid of voxels. Image binarization was then performed by means of supervised thresholds on the gray level histograms, which produced pore and solid phases in white and black, respectively. In order to segment and quantify just the biopores, binary images were processed by applying a "despeckle" procedure (removal of white speckles from the images) set at a value $\leq$ 0.8 mm in order to remove soil matrix porosity. Because the cores were prepared with 2 mm sieved (unstructured) soil, geometrically, the maximum pore diameter between regularly packed 2 mm diameter particles did not exceed 0.8 mm.

2.4. Biopore size distribution characterization

The biopore size distributions (BPSDs) were determined by image

Table 2
Body size parameters of all the inoculated specimens.

Macroinvertebrate groups	Taxa Familia	Body size sequence Individual	Body size parameters Diameter (mm)	Length (mm)	Volume (mm^3)
Earthworms W	Lumbricidae	1	2.8	50.0	307.9
		2	4.2	61.5	893.1
		3	4.7	73.7	1278.6
Millipedes M	Julidae	1	2.3	26.5	109.9
		2	2.6	29.9	158.7
		3	2.8	32.2	198.3
Centipedes C	Geophilidae	1	1.1	48.8	35.7
		2	1.5	61.2	83.2
		3	1.7	69.2	120.8
Campodeiform larvae Cl	Staphylinidae	1	2.6	17.3	91.9
		2	3.6	23.0	234.1
		3	4.1	31.0	409.3
Elateriform larvae El	Elateridae	1	0.8	12.2	6.1
		2	1.3	21.8	28.9
		3	2.5	45.0	220.9

analysis, using the Conmorph software, which was developed at the CNR-ISAFOM, through the application of the 'successive opening' algorithm with spherical 'structuring elements' (e.g., Dougherty & Lotufo, 2003). The effect of this procedure, similar to that used by Capowiez et al. (2003), is exemplified in Fig. 1a and is explained in detail, e.g., in Gargiulo et al. (2015) for two-dimensional images and in Gargiulo et al. (2019) for three-dimensional images. This procedure allows the classification of the entire biopore volume according to the minimum distance between the opposing walls of the pores with a two-voxels-wide increment between each size class. This BPSD statistically represents a population distribution of the pore space produced by the inoculated macroinvertebrates.

The BPSD was first characterized by using mean diameter, standard deviation and the standardized skewness Fisher index , the latter of which being obtained from the BPSD expressed in terms of pore volume percent instead of biopore volume.

2.4.1. *Frequency spectrum analysis of BPSD*

In this work, an index based on the frequency spectrum analysis of the BPSD was introduced in order to search for a more synthetic and powerful parameter able to novelly analyse the shape of the BPSD within the frequency domain. For this purpose, the BPSDs were treated as continuous signals using spline interpolations of original data and, after discrete sampling at 22 points, Fast Fourier Transform (FFT) (Cooley and Tukey, 1965) was applied by using OriginPro (www.OriginLab.com). Then, the following index was calculated for each BPSD:

$$I_{FFT} = \sum_{1}^{N} A_i \tag{1}$$

where A_i is the amplitude of the i-th sinusoids in which the signal is decomposed by FFT and N is half the number of sampling points of the BPSDs.

2.4.2. *Cumulated BPSD Weibull modelling*

The cumulated biopore volume size distributions were modelled by using the Weibull distribution:

$$V(x) = V_t{}^*\left(1 - exp\left[-\left(\frac{x}{\beta}\right)^{\alpha}\right]\right) \tag{2}$$

where $\times$ is the biopore size, $V(x)$ is the cumulated biopore volume having size lower than $\times$, V_b is the total biopore volume, and α and β are the shape and scale parameters of the model, respectively.

The fitting was performed by using Sigmaplot software, version 13.0 (www.systatsoftware.com) and RMSE was recorded as a further parameter to characterize BPSDs.

2.5. *Prediction potential of BPSD parameters on soil macroinvertebrate morphotype*

For each BPSD parameter, two factor ANOVA without replication

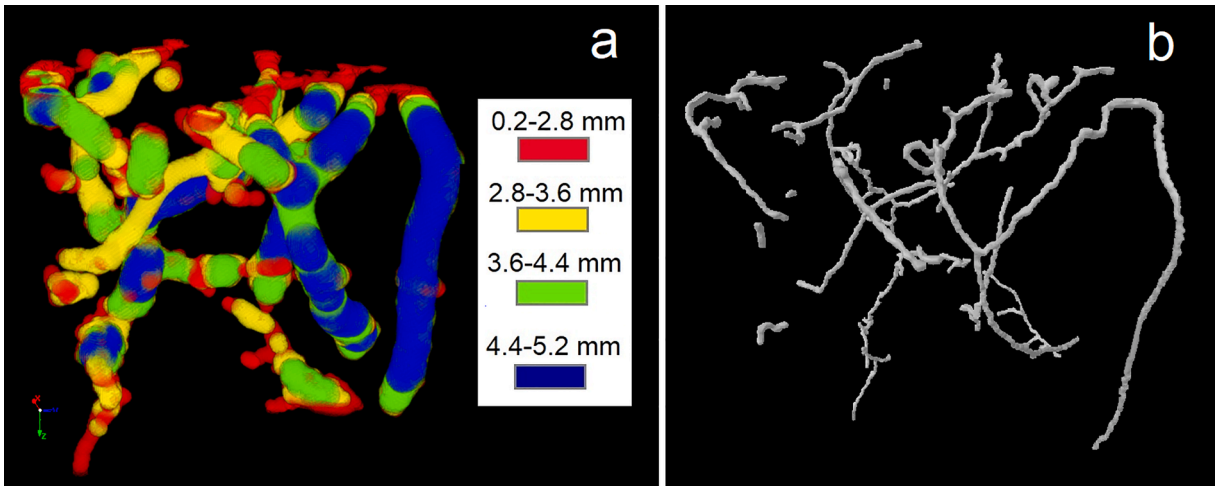

Fig. 1. Effects of biopore image analysis procedures: a) Pore size distribution, example of color coded biopore volume according to pore diameter; b) Skeletonization of the biopore system to calculate topological parameters.

was performed to check whether taxa and body size were sources of variation, making the implicit assumption that there is no interaction between the two factors. Next, Fisher LSD tests were performed to check significant differences for all couples of both taxa and body sizes. These statistical tests were performed at $\alpha = 0.05$ significance by using Sigmaplot software, version 13.0 (www.systatsoftware.com).

Discriminant Analysis (DA) was performed as a probabilistic classifier by using the taxa as grouping variables and two distinct sets of BPSD parameters as independent predictor variables. The first set of parameters was determined directly from the population distribution provided by the image analysis procedure, while the second was obtained from the Weibull modelling of the cumulated version of the BPSDs. DA was carried out with the assumption of a common within-group covariance matrix, producing linear decision boundaries of group-membership (Tharwat, 2016). DA was carried out with the use of SPSS software version 26.0 (www.ibm.com).

2.6. Topological characterization of galleries

As some of the inoculated soil macroinvertebrates produce galleries, the topology of their structure was also characterised by determining the 3D skeleton of the bio-pore space. An example is shown in Fig. 1b. The image skeletonization process was performed on the binarized images by applying the 3D thinning algorithm (Lee et al., 1994) to the gallery systems using Image J software (https://imagej.nih.gov/ij/). The gallery system of a mesocosm consists of all the distinct galleries found therein. The 3D skeleton represents the medial axis of the gallery system of each mesocosm and consists of sets of segments joined by junction points. Each of these sets corresponds to a distinct gallery. The rank of a junction point is the number of segments joined at that point. The tortuosity of each distinct gallery is the ratio between the sum of the lengths of the segments of the shortest path of that gallery and the Euclidean distance between the ends of this shortest path. The following topological parameters were then computed for each mesocosm:

- Length: sum of the lengths of all segments of the gallery system.
- Longest shortest path length: average length of the longest of the shortest paths of the unconnected galleries weighted according to their lengths.
- Tortuosity: average tortuosity of the longest of the shortest paths of the distinct galleries weighted according to their lengths.
- Vertical deviation: average vertical deviation of all the segments in the gallery system weighted according to their lengths.
- Rate of branching: ratio between the total number of the gallery segment junctions and the gallery system length.
- Junction rank: mean value of the junction rank distribution calculated from the whole gallery system.

In addition to the BPSD parameters, two factor ANOVA and Fisher LSD tests were also performed for the above topological parameters.

3. Results

The Fig. 2 shows an example of the 3D visualization of the biopores obtained. The animals shown represent the individuals which produced the corresponding biopores. The largest inoculated specimen was the Earthworm 3 while the smallest was the Elateriform larva 1. The segmentation procedures applied to 3D images of the mesocosms allowed the burrowing activity of all the groups to be visualized adequately. All of the 15 reconstructed biopore systems are shown in Supplementary figure 1, from which it can be particularly noted that the burrowing activity of Centipedes and Campodeiform larvae did not result in visible galleries. Moreover, Campodeiform larvae produced large chambers mainly at the base of the mesocosms.

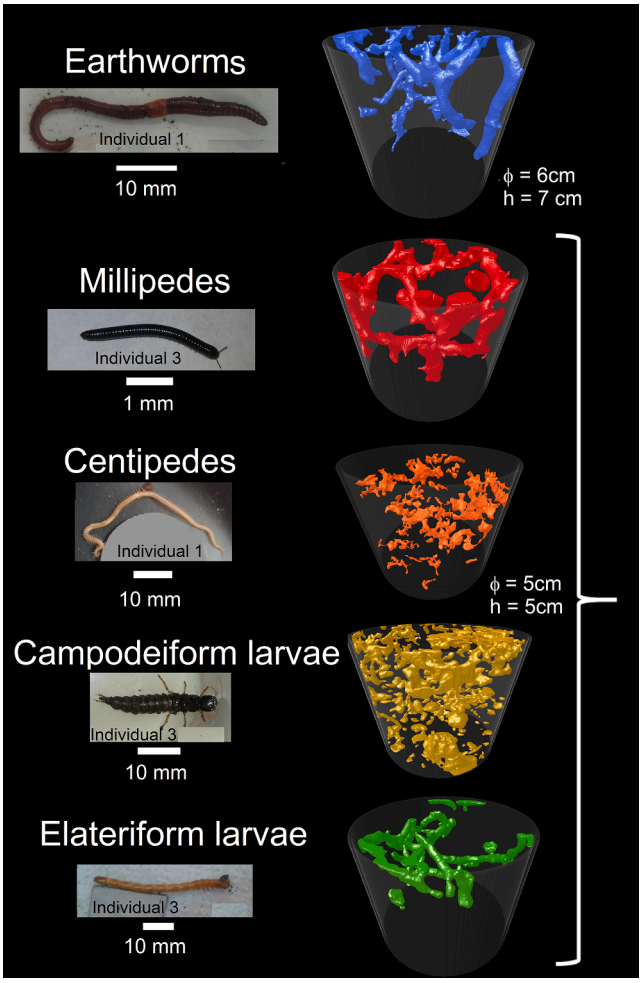

Fig. 2. Examples of inoculated macroinvertebrates and 3D reconstructions of the produced biopores. Φ and h are diameter and height of the soil cores, respectively. Cores do not appear cylindrical because of the perspective.

3.1. Biopore size distribution characterization

Fig. 3 shows the size distributions of the segmented biopores in which each size class was 0.4 mm wide, which is the twice the voxel size. Indeed, one voxel is the minimum radius increment of the spherical structuring elements which are used in the mathematical morphology algorithm applied here. The biopore size distributions of the three individuals in each macroinvertebrate group are reported in each graph.

A preliminary visual examination permits us to observe that the BPSDs of Earthworms (W) and Campodeiform larvae (Cl) are multimodal, those of Millipedes (M) are bimodal, and those of Centipedes (C) and Elateriform larvae (El) are unimodal. Comparison of the BPSDs of the three individuals within each macroinvertebrate group shows a very similar shape for C and El.

3.1.1. Parameters from the population distribution

Table 3 shows the parameters calculated on the basis of the population distributions (Fig. 3). Average values for each macroinvertebrate group are also reported. All the biopore data are reported in the Supplementary file S1.

Average total biopore volumes were significantly different between all the groups, with W exhibiting the largest volume and El the smallest one. The order of the average total biopore volumes corresponds to that of average body volume of the inoculated macroinvertebrate groups.

The mean diameter of the W biopores was the largest and was significantly different from those of the biopores of the other groups. The

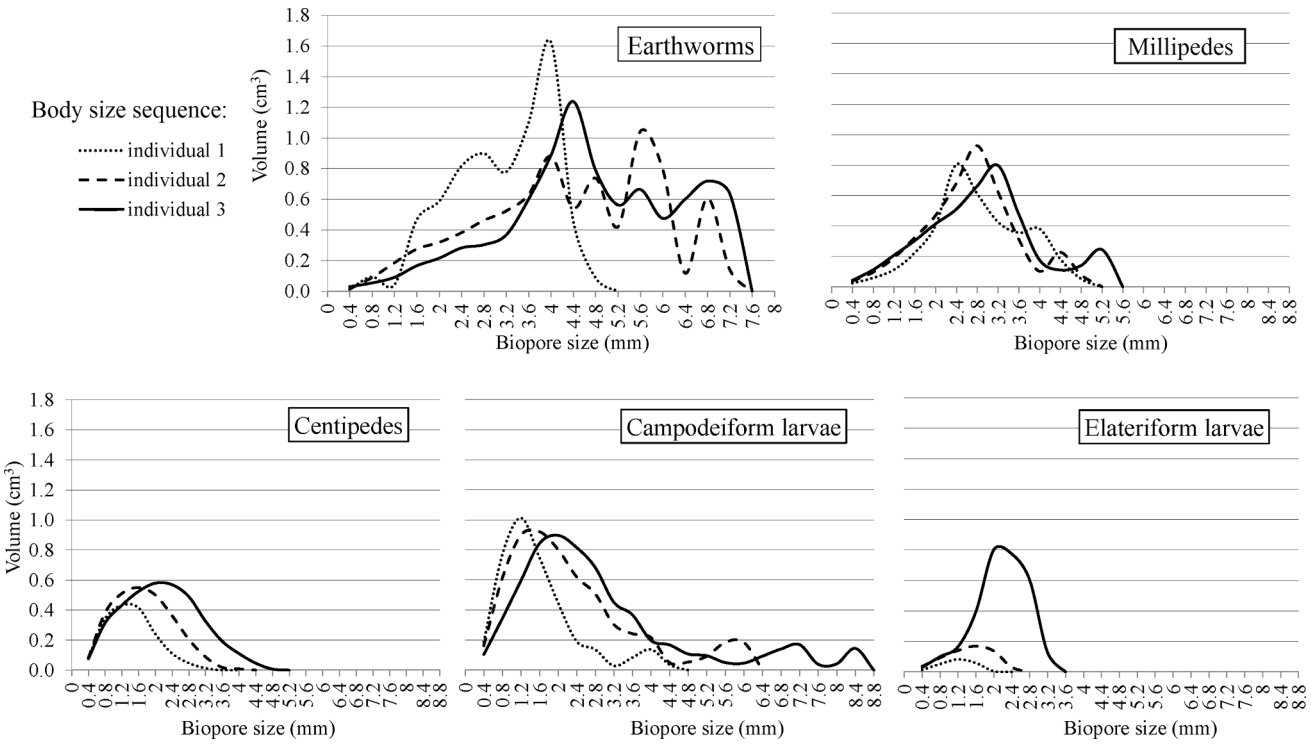

Fig. 3. Biopore size distributions of soil macroinvertebrates.

Table 3
Parameters of soil macroinvertebrate biopore size distribution. Average (Avg.) values sharing letters along column are not significantly different (Fisher LSD method) at a $p < 0.05$.

Macroinvertebrate group	Body size sequence	Biopore volume (mm^3)	Mean diameter (mm)	Standard deviation mm	Skewness index Fisher [a]	FFT index [a]
Earthworms W	1	6.96	3.15	0.89	−0.466	0.100
	2	8.15	4.37	1.57	−0.257	0.098
	3	8.67	4.76	1.54	−0.283	0.089
	Avg.	7.93a	4.09a	1.34a	−0.335c	0.096a
Millipedes M	1	3.63	2.81	0.89	0.014	0.081
	2	4.06	2.68	0.89	0.063	0.083
	3	4.19	2.90	1.08	0.199	0.084
	Avg.	3.96c	2.80b	0.95b	0.092b	0.083b
Centipedes C	1	1.69	1.43	0.58	0.471	0.060
	2	2.71	1.72	0.71	0.345	0.061
	3	3.67	2.17	0.91	0.242	0.054
	Avg.	2.69d	1.77 cd	0.73bc	0.353b	0.058c
Campodeiform larvae Cl	1	3.78	1.57	0.86	1.370	0.100
	2	5.85	2.29	1.36	1.142	0.084
	3	6.39	2.90	1.83	1.382	0.111
	Avg.	5.34b	2.25bc	1.35a	1.298a	0.098a
Elateriform larvae El	1	0.21	1.18	0.37	−0.248	0.046
	2	0.60	1.44	0.51	−0.210	0.038
	3	2.99	2.16	0.58	−0.561	0.064
	Avg.	1.27e	1.60d	0.49c	−0.340c	0.050c

[a] Parameter for which two factor Anovas provided that individual body size is not a source of variation

order of average biopore mean diameters does not correspond to that of body diameters of the macroinvertebrate individuals. Average biopore mean diameters are always slightly larger than the average body diameters, except in the Cl group, where notwithstanding the presence of very large pores (chambers) (see Fig. 2), the pore mean diameter is smaller than the body diameter.

The average standard deviations of W and Cl were significantly larger than those of other groups. The standard deviation values are an indicator of the width of the pore size range and the large values of W and Cl correspond to the multimodality, the intermediate value of M to the bimodality and the smaller values of C and El to the unimodal behaviour of their BPSDs.

The standardized skewness index was negative for both W and El with no significantly different values. Cl had the significantly largest index, followed by M and C.

Regarding the FFT index, macroinvertebrate groups (W and Cl) with multimodal BPSDs did not show values that were significantly different from one another, but they were significantly different from that of the group (M), which has bimodal BPSD. This in turn was significantly different from the FFT indices of the groups (C and El) with unimodal BPSDs (see Fig. 3) and, in addition, the indices of these two groups did not differ significantly from one another. Complete input and output

data of the discrete Fourier transform on which the FFT index is based are reported in Supplementary file S2 and in Supplementary figure 3.

The results of two factor ANOVAs (see Supplementary file S4), performed on all of the parameters reported in table 3, showed that the body size sequence was not a source of variation for the Skewness and FFT indices.

3.1.2. Parameters from Weibull modelling of cumulated distributions

Table 4 shows some parameters obtained from the Weibull modelling. Average values for each macroinvertebrate group are also reported (overall results are in the Supplementary file S3). Fig. 4 shows the fitted curves with the confidence and prediction bands.

The average α shape parameters of W, M and El were larger than 3 and significantly larger than those of C and Cl. This means that the cumulated BPSDs of W, M and Cl approximate a sigmoidal function better than those of C and Cl, which are more similar to DCS (downward concave shape) functions.

The value of the β scale parameter increased according to the body size sequence within each macroinvertebrate group. W exhibited the significantly largest average value followed by that of M, which in turn was significantly larger than those of C, Cl and El.

W and Cl showed the significantly largest value of average RMSE, followed by that of M, which had a value that was significantly larger than those of C and El.

A two factor ANOVA was also performed on the parameters reported in table 4 and indicated that the body size sequence was not a source of variation for the shape parameter α and RMSE.

3.2. Prediction potential of BPSD parameters on soil macroinvertebrate morphotypes

An evaluation of the prediction potential of the set of the calculated parameters for identification of the macroinvertebrate group producing a given BPSD was carried out. The prediction potentials obtainable from both approaches used for the BPSD characterization were evaluated separately. In particular, we performed two bivariate analyses in which the Skewness and FFT indices were considered as predictors of the morphotype group membership for the first approach and shape parameter α and RMSE for the second.

Table 4
Parameters and fitting performance of Weibull modelling of cumulated biopore size distribution. Average (Avg.) values sharing letters along column are not significantly different (Fisher LSD method) at a $p < 0.05$.

Macroinvertebrate group	Body size sequence	α[a]	β	RMSE[a]
Earthworms W	1	3.673	3.318	0.235
	2	2.875	4.764	0.212
	3	3.261	5.140	0.201
	Avg.	3.270a	4.407a	0.216a
Millipedes M	1	3.222	2.912	0.071
	2	3.269	2.769	0.077
	3	2.835	3.025	0.095
	Avg.	3.109a	2.902b	0.081b
Centipedes C	1	2.272	1.386	0.007
	2	2.258	1.725	0.016
	3	2.285	2.242	0.031
	Avg.	2.272b	1.784c	0.018c
Campodeiform larvae Cl	1	1.809	1.475	0.115
	2	1.596	2.279	0.146
	3	1.583	2.874	0.238
	Avg.	1.663b	2.209c	0.166a
Elateriform larvae El	1	3.082	1.111	0.004
	2	2.706	1.430	0.015
	3	4.140	2.191	0.046
	Avg.	3.309a	1.577c	0.022c

[a] Parameter for which two factor Anovas provided that individual body size is not a source of variation

Fig. 5 shows the score plots obtained from the Discriminant Analysis performed considering the macroinvertebrate groups as grouping variables. The separation boundaries of the membership regions are also reported and they were linear as the hypotheses of equal population covariance matrices within groups were satisfied (see Supplementary file S5).

Discriminant functions DF1 and DF2 explained 86.5% and 13.5% of variable variance, respectively with population distribution parameters (Fig. 5a), and 72.1% and 27.9% using Weibull model parameters (Fig. 5b).

All scores lie in the respective membership region in Fig. 5a, while one of the scores corresponding to the El group lies in the C membership region in Fig. 5b.

Overall classification results are summarised in table 5. The use of Skewness and FFT indices led to 100% of all the group memberships being correctly predicted, while the use of Weibull model parameters α and RMSE provided 100% of group membership being correctly predicted only for 4 groups. Indeed, only 66.7% of group membership was correctly predicted for El. This last result corresponds to an overall 93.3% of group membership correctly classified by using Weibull model parameters.

3.3. Topological characterization of galleries

For the three macroinvertebrate groups producing galleries, the topological parameters calculated are reported in table 6. Average length of the biopore gallery systems did not show a significant difference between the macroinvertebrate groups. An increasing trend with the body size for El and a decreasing one with body size for M were observed. The tortuosity was the significantly lowest for El and, along with M, showed increasing values with increasing body size. Vertical deviation of the gallery system was significantly lowest for W and a two factor ANOVA indicated that the body size sequence was not a source of variation for this parameter. Neither the rate of branching nor junction rank differed significantly between the macroinvertebrate groups, and they showed an increasing and decreasing trend with the body size for M and El larvae, respectively.

Regarding the most evident relationships between the topological parameters, it can be noted (see also the scatter plot matrix in Supplementary figure 2) that the tortuosity for El shows a positive linear trend with respect to the length. Both tortuosity and length exhibit a decreasing trend with respect to the remaining parameters. For M, the tortuosity, the rate of branching and the junction rank show a decreasing linear trend with respect to the length. The tortuosity shows an increasing trend with junction rank.

4. Discussion

In this work, the mesocosm incubation was carried out in the field in order to place the soil macroinvertebrates in their natural range of temperature, light and humidity conditions as much as possible. Using such an approach, the inoculated individuals left evidence of their burrowing activity in all soil mesocosms that underwent X-ray tomography. The de-speckle pre-processing that was applied to the images permitted us to isolate exclusively biopores from the 3D reconstruction of the repacked cores (see Fig. 2 and Supplementary figure 1). The unexpected absence of visible galleries within all of the mesocosms inoculated with Centipedes and Campodeiform larvae could be due to the specific burrowing mechanisms used by these macroinvertebrates. Actually, Centipedes push their bodies into the soil by using their short feet as anchors and Campodeiform larvae are very active and energic in using their strong and well-developed thoracic legs when moving forward in the substrate (Orth et al., 1975). It could be argued that these behaviours result in galleries with less compacted walls which are, thus, less stable than those of the other three studied morphotypes.

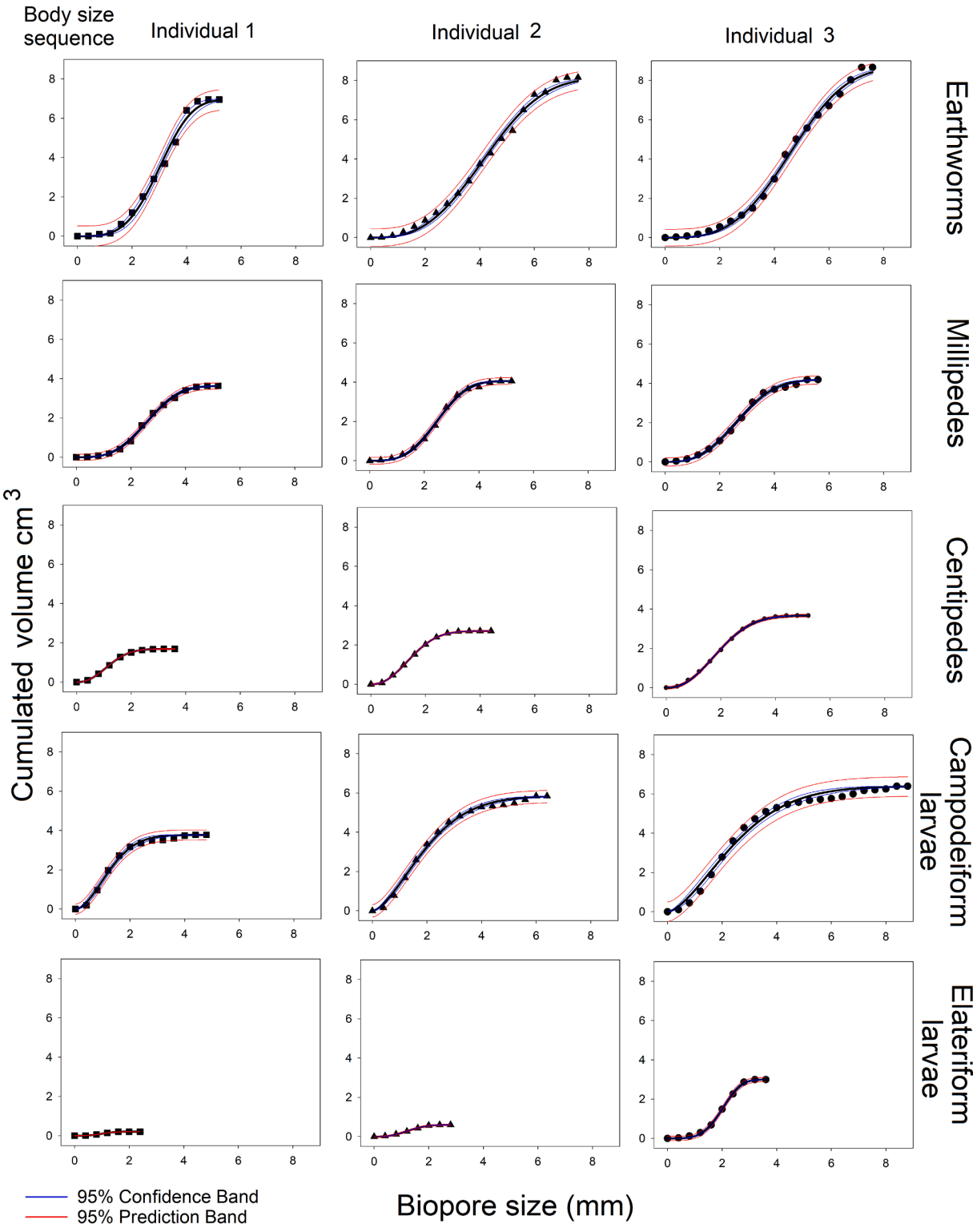

Fig. 4. Weibull model fitting of cumulated biopore size distributions.

4.1. Biopore size distribution characterization

The multiplicity of the modes in the BPSDs shown in Fig. 3 has different origins due to the different burrowing behaviour of the macroinvertebrate groups. The many modes of BPSDs of W are due to galleries of different diameters, the largest of which are those free of casts, while the smaller ones are those that are partially cast coated. The largest modal values are larger than the average W body diameter, most probably because the gallery diameter corresponds to the larger diameter of a segment of the earthworm which contracted during its peristaltic movement (e.g., Ruiz and Or, 2018; Calderon et al., 2019). Among the multiple BPSDs modal values of Cl, the larger are those corresponding to the diameter of the few, but very large, chambers they usually produce (Lipkow and Betz, 2005). Finally, the largest modal value of the bimodal BPSDs of M corresponds with the typical spiral-shaped chambers produced when M are in their curled position

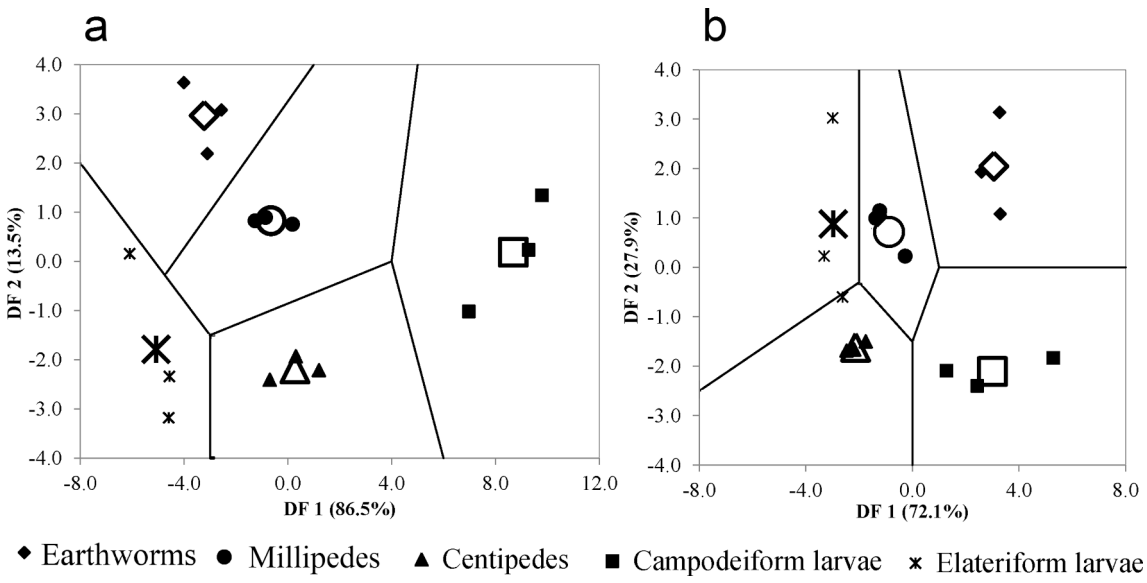

Fig. 5. Score plots of DA with membership regions using (a) population distribution parameters and (b) Weibull model parameters. Larger symbols are centroids of the scores.

Table 5
Classification results of DA applied to Skewness and FFT indices of BPSD. In brackets are results of DA applied to shape and RMSE parameters obtained from BPSD Weibull modelling.

Macroinvertebrate group		Predicted group membership [a]					Original
		W	J	C	Cl	El	
Count	W	3	0	0	0	0	3
	M	0	3	0	0	0	3
	C	0	0	3	0	0	3
	Cl	0	0	0	3	0	3
	El	0	0	0(1)	0	3(2)	3
%	W	100	0	0	0	0	100
	M	0	100	0	0	0	100
	C	0	0	100	0	0	100
	Cl	0	0	0	100	0	100
	El	0	0	0(33.3)	0	100(66.7)	100

[a] 100% (93.3%) of original grouped cases correctly classified.

(Bowen and Hembree, 2014). Unimodal BPDSs of C and El are the result of two different burrowing behaviours, as El produced galleries while C did not.

4.1.1. Parameters from the population distribution

The skewness and the FFT indices are the BPSD shape parameters considered in this study. The sign of the skewness index is an indicator of the relative predominance of small (e.g., for Cl) or large (e.g., for W) pores in the biopore system. The FFT index is a novel parameter proposed in this study to characterize the BPSDs. Observation of significant differences of such parameters obtained for the different macroinvertebrates suggests that FFT index could be a reliable indicator of the presence or absence of multiple modes in the BPSDs. Skewness and FFT indices are related only to the shape of BPSDs and the results of two-factor ANOVAs indicate that the body size sequence isn't a source of variation for such indices. Therefore, they are suitable to represent the burrowing geometries of a given macroinvertebrate group independently from the size of the individuals.

4.1.2. Parameters from Weibull modelling of cumulated distributions

The fitting of the cumulated BPDSs with Weibull model was, in general, very good ($R^2 > 0.993$ in all cases) confirming the findings of Neithalath et al. (2010) and Xiong et al. (2017), which applied the same model on size distributions of macropores calculated using exactly the same image analysis procedure applied in this work with comparable image resolution and pore size range.

Results suggest that the β parameter could be considered an indicator

Table 6
Topological parameters of the skeleton of biopore system for macroinvertebrate groups burrowing galleries. Average (Avg.) values sharing letters along column are not significantly different (Fisher LSD method) at a $p < 0.05$.

Macroinvertebrate group	Body size sequence	Burrow topology Length (mm)	Tortuosity	Vertical deviation [a](°)	Rate of branching (number/cm)	Junction rank
Earthworms W	1	547.46	3.39	30.70	1.14	3.08
	2	211.54	7.09	17.47	0.85	3.06
	3	595.92	6.94	29.00	1.96	3.10
	Avg.	451.64	5.81a	25.72b	1.32	3.08
Millipedes M	1	817.62	4.96	84.72	0.77	3.02
	2	641.17	6.87	72.36	0.86	3.06
	3	520.92	7.63	69.78	0.92	3.10
	Avg.	659.90	6.49a	75.62a	0.85	3.06
Elateriform larvae El	1	180.50	2.07	81.01	0.94	3.12
	2	287.24	3.42	74.34	0.85	3.08
	3	473.82	5.08	61.85	0.63	3.03
	Avg.	313.85	3.52b	72.40a	0.81	3.08

[a] Parameter for which two factor Anovas provided that individual body size is not a source of variation

of the body size of the animals, differently from α and RMSE, which can be considered independent from body size.

As observed for the FFT index, the RMSE parameter resulted a good indicator of the presence or absence of multiple modes in the original pore population distributions. On the other hand, such results were expected because Weibull is a unimodal distribution model, which poorly fits multi- or bimodal data distributions, and then RMSE consequently increases. In particular, the prediction bands shown in Fig. 4 indicate that the model does not fit well especially at the large biopore size classes in the case of Cl, and at both small and large biopore size classes in the case of W.

4.2. Prediction potential of BPSD parameters on soil macroinvertebrate morphotype

Both of the score plots obtained from the Discriminant Analysis (Fig. 5) show that the membership region of M is central, thus it is more limited and smaller than the other regions. Such a limited domain for the discriminant function values characterizing the M membership could be related to the peculiar bimodality of the BPSDs of M. Moreover, the classification results reported in table 5 indicate that biopores of El were the most difficult to recognise.

In general, results of DA demonstrated that BPSDs contain sufficient information to recognize the morphotype group of the soil macroinvertebrates that produces the corresponding biopore system. In particular, the use of BPSD parameters obtained from image analysis fully succeeded in group membership prediction and a very good result was obtained also when modelling the BPSD with Weibull distribution. The slight difference in prediction potential between the two BPSD parameterization approaches can be explained by the fact that the modelling of the original data provided by pore image analysis simplifies, but necessarily produces a loss of information. On the other hand, Weibull modelling of BPSDs can be useful for modeling water retention close to the saturation point as the Weibull parameters can themselves be used as parameters of a water retention function as demonstrated in Appendix A.

Overall, DA of BPSD parameters can be considered very promising, for example, in neoichnological studies (e.g., Hembree, 2016). On the other hand, the good result found in group membership prediction means that each soil macroinvertebrate morphotype produces a very specific pore size distribution i.e., a typical impact on soil structure. Therefore, most advanced models of soil structure dynamics induced by soil fauna activity (e.g. Meurer et al., 2020), which usually refer only to earthworms, would perform better if they were specifically calibrated for burrowing activity of a range of soil macroinvertebrates.

4.3. Topological characterization of galleries

Topological parameters calculated for W, M and El galleries showed some correlations depending on the morphotype group and all parameters were related to the size of the inoculated individuals except for the vertical deviation, which was independent from the body size sequence. An improved version of such a parameter with respect to the original definition of Capowiez et al. (2011) was used in this study in order to obtain a quantitative characterization of vertical deviation of the entire gallery system that better corresponded to its visual observation. An analogous but different approach to describe the orientation of the gallery system was used by Bottinelli et al. (2017) that weighted the orientation of max Feret diameters of the pore objects with their volume. In the present work, the vertical deviation of each gallery segment was instead weighted with its length, obtaining an average vertical deviation for the gallery system skeleton. In the case, for example, of anecic earthworms that produce very long vertical galleries sometimes connected with horizontal gallery segments, the average vertical deviation, calculated without taking into account for the length of the individual galleries, would give rise to a value much higher, i.e, more subhorizontal, than that corresponding to the real burrowing activity and the visual observation. In general, the values obtained with this approach can be considered representative of the prevailing direction of the burrowing activity. This pursues the objective of developing new traits useful for assigning the ecological category of earthworm species, based not only on their morpho-anatomical characteristics, as suggested by Bottinelli et al. (2020).

5. Conclusions

The soil fauna inoculum experiment carried out in this work using five different groups of macroinvertebrates reduces a gap existing in the characterisation of the biopores produced by soil fauna burrowing activity, which is mainly focused on the study of earthworm biopores. The specific contributions to the soil biopore system of five macroinvertebrate morphotypes exhibiting different burrowing mechanisms have been considered one at time in this preliminary study. Further investigation through mesocosm inoculation with combinations of different macroinvertebrate groups will, of course, be needed in order to study the prediction potential of BPSD parameters in recognising soil fauna communities that produce the biopore systems in natural soils.

Determining soil BPSDs by means of non-destructive 3D imaging has proven itself effective for accurate characterisation of biopore systems and both BPSD parameterization approaches proposed in this work yielded successful results. The approach based on direct analysis of BPSDs obtained through mathematical morphology was the most effective in DA for predicting macroinvertebrate group membership on the basis of the characterization of their burrows, while the other, based on Weibull modelling of cumulated BPSDs, proved more advantageous for modelling water retention in those macropores. The most effective for group membership prediction were the BPSD parameters independent from macroinvertebrate body size, such as the skewness and FFT indices obtained from the first approach and the Weibull shape parameter α from the second one. In particular, the novel parameter FFT index introduced here proved effective in quantifying the BPSD multimodality synthetically and, thus, the complexity of the entire soil pore system.

Overall, the effectiveness of the FFT index as an indicator of BPSD complexity and the advantages of Weibull modelling described in this study are actually generally valid for any kind of soil pore size distribution that is determined by imaging methods, which have to be three-dimensional in the case of Weibull modelling. Moreover, the discriminant analysis, applied here for the first time on BPSD data, could be considered a promising soil structure investigation approach which is suitable for many other prediction purposes. Indeed, DA could be applied by using many other soil structure formation factors besides macroinvertebrate morphotypes as grouping variables. Overall, the approach of soil pore investigation proposed in this work can be seen as a further tool that is available for enhancing studies of the relationships between soil management and its impact on soil pore systems.

Declaration of Competing Interest

The authors declare that they have no known competing financial interests or personal relationships that could have appeared to influence the work reported in this paper.

Acknowledgment

The authors want to thank Dr Luciana Minieri of the Department of Agriculture, University of Napoli Federico II, for the soil chemical analysis and Nadia Orefice of the Institute for Agricultural and Forest Systems in the Mediterranean (ISAFoM), CNR, for the soil granulometric analysis.

This research did not receive any specific grant from funding agencies in the public, commercial, or nonprofit sectors.

Appendix A

Starting from studies of the geometry of multicomponent sphere packs, for the pore volume probability distribution, Assouline et al. (1998) derived the general expression:

$$F\left(v_p^{'}\right) = 1 - \exp\left(- \frac{v_p^{'a}}{\beta}\right) \qquad (1)$$

$$v_p^{'} = \left(v_p - v_{pmin}\right)/\left(v_{pmax} - v_{pmin}\right)$$

which is a Weibull distribution, with α and β being the shape and scale parameters, respectively. For $v_p = v_{pmin}$, $F(v_p) = 0$. When $v_p = v_{pmax}$, $F(v_p) \rightarrow 1$ at a rate that depends on the value of β. When all the pore volume, up to v_{pmax} is filled with water, the soil water content θ is equal to θ_s, and $Se = (\theta\text{- }\theta_r)/(\theta_s\text{ - }\theta_r) = 1$, with θ_r being the residual volumetric water content. When all the pores are filled with air, the soil water content is equal to θ_r, and $Se = 0$. Therefore (1) can also represent the effective saturation function:

$$S_e\left(v_p^{'}\right) = 1 - \exp\left(- \frac{v_p^{'a}}{\beta}\right) \qquad (2)$$

$$v_p^{'} = \left(v_p - v_{pmin}\right)/\left(v_{pmax} - v_{pmin}\right)$$

Every pore volume portion, v_p, has two specific capillary heads below which it drains or fills with water, ψ_d and ψ_w. In the following, we will consider just the drying process, but the approach is also applicable to the wetting phase in order to account for the hysteresis in the water retention curves. A relationship between v_p and ψ can be formulated when the equation of capillarity is applied to pores. Each pore volume portion, as it is fractioned by the mathematical morphology image analysis procedure applied here for the BPSD calculation, can be represented by a spherical volume of radius r, that is:

$$v_p = 4/3\pi r^3 \qquad (3)$$

The radius, r, is then related to the capillary head, ψ, by

$$r = -c\psi^{-1} \qquad (4)$$

where c is a parameter which depends on the liquid tension and the contact angle between liquid and solid. At a given ψ, all the pore space portions with radius smaller than or equal to the corresponding $r(\psi)$ value (equation 4) are saturated with water, while all the pore portions with larger radii are empty. Therefore, replacing (3) and (4) with (2) leads to the definition of the relationship between S_e and ψ:

$$S_e(\psi) = 1 - exp\left[-\beta^{-1}\left(\frac{\psi^{-3} - \psi_{min}^{-3}}{\psi_{max}^{-3} - \psi_{min}^{-3}}\right)^{\alpha}\right] \qquad (5)$$

Assuming $\psi_{\max} = 0$ and $\psi_{\min} = \psi_R$ in equation (5), where R is the image resolution (voxel size) and ψ_R the capillary head corresponding to the radius $r = R$ (equation 4), we obtain the following water retention curve based on the *a priori* knowledge of the macropore size distribution:

$$\theta(\psi) = (\theta_s - \theta_R)\left\{1 - exp\left[-\beta^{-1}\left(\frac{\psi^{-3} - \psi_R^{-3}}{\psi_R^{-3}}\right)^{\alpha}\right]\right\} + \theta_R \qquad (6)$$

where α and β are the parameters obtained from Weibull modelling of the BPSDs calculated through the image analysis and θ_R corresponds to the biopore volume portion with a radius lower than resolution (R) thus not detectable by image analysis. The fundamental advantage of (6) in comparison to other widely used water retention models is that the parameters are directly available from pore image analysis.

In particular, considering resolution (0.2 mm) of the images in this work and standard conditions for temperature, pressure and surface tension of water and contact angle of water with pore wall equal to zero, Jurin's law (4) leads the equation (6) to describe biopore water content for the range $0 \geq \psi \geq$ -14.8 cm of capillary heads.

Appendix B. Supplementary data

Supplementary data to this article can be found online at https://doi.org/10.1016/j.geoderma.2021.115292.

References

Assouline, S., Tessier, D., Bruand, A., 1998. A conceptual model of the soil water retention curve. Water Resour. Res. 34 (2), 223–231. https://doi.org/10.1029/97wr03039.

Baccaro, M., Harrison, S., van den Berg, H., Sloot, L., Hermans, D., Cornelis, G., van Gestel, C.A.M., van den Brink, N.W., 2019. Bioturbation of Ag2S-NPs in soil columns by earthworms. Environ. pollut. 252, 155–162. https://doi.org/10.1016/j.envpol.2019.05.106.

Balseiro-Romero, M., Mazurier, A., Monoshyn, D., Baveye, P.C., Clause, J., 2020. Using X-ray microtomography to characterize the burrowing behaviour of earthworms in heterogeneously polluted soils. Pedobiologia 83, 150671. https://doi.org/10.1016/j.pedobi.2020.150671.

Bastardie, F., Capowiez, Y., Cluzeau, D., 2005. 3D characterisation of earthworm burrow systems in natural soil cores collected from a 12-year-old pasture. Appl Soil Ecol 30 (1), 34 46. https://doi.org/10.1016/j.apsoil.2005.01.001.

Bastardie, F., Capowiez, Y., De Dreuzy, J.R., Cluzeau, D., 2003. X-ray tomographic and hydraulic characterization of burrowing by three earthworm species in repacked soil cores. Appl Soil Ecol 24 (1), 3–16. https://doi.org/10.1016/s0929-1393(03)00071-4.

Bottinelli, N., Hedde, M., Jouquet, P., Capowiez, Y., 2020. An explicit definition of earthworm ecological categories–Marcel Bouché's triangle revisited. Geoderma 372, 114361. https://doi.org/10.1016/j.geoderma.2020.114361.

Bottinelli, N., Zhou, H., Capowiez, Y., Zhang, Z.B., Qiu, J., Jouquet, P., Peng, X.H., 2017. Earthworm burrowing activity of two non-Lumbricidae earthworm species incubated in soils with contrasting organic carbon content (Vertisol vs. Ultisol). Biol Fert Soils 53 (8), 951–955. https://doi.org/10.1007/s00374-017-1235-8.

Bowen, J.J., Hembree, D.I., 2014. Neoichnology of two spirobolid millipedes: improving the understanding of the burrows of soil detritivores. Palaeontol Electron 17 (1), 1–48. https://doi.org/10.26879/395.

Capowiez, Y., Bottinelli, N., Sammartino, S., Michel, E., Jouquet, P., 2015. Morphological and functional characterisation of the burrow systems of six earthworm species

(Lumbricidae). Biol Fert Soils 51 (7), 869–877. https://doi.org/10.1007/s00374-015-1036-x.
Capowiez, Y., Sammartino, S., Michel, E., 2014. Burrow systems of endogeic earthworms: Effects of earthworm abundance and consequences for soil water infiltration. Pedobiologia 57 (4), 303–309. https://doi.org/10.1016/j.pedobi.2014.04.001.
Capowiez, Y., Sammartino, S., Michel, E., 2011. Using X-ray tomography to quantify earthworm bioturbation non-destructively in repacked soil cores. Geoderma 162 (1), 124–131. https://doi.org/10.1016/j.geoderma.2011.01.011.
Capowiez, Y., Pierret, A., Moran, C.J., 2003. Characterisation of the three-dimensional structure of earthworm burrow systems using image analysis and mathematical morphology. Biol Fert Soils 38 (5), 301–310. https://doi.org/10.1007/s00374-003-0647-9.
Cheik, S., Bottinelli, N., Minh, T.T., Doan, T.T., Jouquet, P., 2019. Quantification of three dimensional characteristics of macrofauna macropores and their effects on soil hydraulic conductivity in northern Vietnam. Front. Environ. Sci. 7, 31. https://doi.org/10.3389/fenvs.2019.00031.
Cooley, J.W., Tukey, J.W., 1965. An algorithm for the machine calculation of complex Fourier series. Math Comput 19 (90), 297–301. https://doi.org/10.1090/s0025-5718-1965-0178586-1.
Daniel, O., Kretzschmar, A., Capowiez, Y., Kohli, L., Zeyer, J., 1997. Computer-assisted tomography of macroporosity and its application to study the activity of the earthworm Aporrectodea nocturna. Eur. J. Soil Sci. 48, 727–737. https://doi.org/10.1111/j.1365-2389.1997.tb00572.x.
Dougherty, E. R., Lotufo, R. A., 2003. Hands-on morphological image processing (Vol. 59). SPIE press. 10.1117/3.501104.
Drager, K.I., Hirmas, D.R., Hasiotis, S.T., 2016. Effects of Ant (Formica subsericea) Nests on Physical and Hydrological Properties of a Fine-Textured Soil. Soil Sci Soc Am J 80 (2), 364–375. https://doi.org/10.2136/sssaj2015.08.0300.
Gargiulo, L., Mele, G., Terribile, F., 2015. The role of rock fragments in crack and soil structure development: a laboratory experiment with a Vertisol. Eur. J. Soil Sci. 66 (4), 757–766. https://doi.org/10.1111/ejss.12263.
Gargiulo, L., Grimberg, Å., Repo-Carrasco-Valencia, R., Carlsson, A.S., Mele, G., 2019. Morpho-densitometric traits for quinoa (Chenopodium quinoa Willd.) seed phenotyping by two X-ray micro-CT scanning approaches. J Cereal Sci 90, 102829. https://doi.org/10.1016/j.jcs.2019.102829.
Helliwell, J.R., Sturrock, C.J., Grayling, K.M., Tracy, S.R., Flavel, R.J., Young, I.M., Whalley, W.R., Mooney, S.J., 2013. Applications of X-ray computed tomography for examining biophysical interactions and structural development in soil systems: a review. Eur. J. Soil Sci. 64 (3), 279–297. https://doi.org/10.1111/ejss.12028.
Hembree, D., 2016. Using experimental neoichnology and quantitative analyses to improve the interpretation of continental trace fossils. Ichnos 23 (3–4), 262–297. https://doi.org/10.1080/10420940.2016.1202684.
IUSS Working Group WRB 2014. World Reference Base for Soil Resources 2014. International Soil Classification System for Naming Soils and Creating Legends for Soil Maps. World Soil Resource Report No 106, FAO, Rome.
Jones, C.G., Lawton, J.H., Shachak., M., 1994. Organisms as ecosystem engineers. Oikos 69:373–386. 10.2307/3545850.
Joschko, M., Muller, P.C., Kotzke, K., Dohring, W., Larink, O., 1993. Earthworm burrow system development assessed by means of X-ray computed tomography. Geoderma 56, 209–221. https://doi.org/10.1016/0016-7061(93)90111-w.
Khan, M. A., Ahmad, W., Paul, B., 2018. Ecological impacts of termites. In Termites and Sustainable Management (201-216). Springer, Cham. 10.1007/978-3-319-72110-1_10.
Kime, R.D., Golovatch, S.I., 2000. Trends in the ecological strategies and evolution of millipedes (Diplopoda). Biological Journal of the Linnean Society 69 (3), 333–349. https://doi.org/10.1111/j.1095-8312.2000.tb01209.x.
Kuzyakov, Y., Blagodatskaya, E., 2015. Microbial hotspots and hot moments in soil: concept & review. Soil Biol Biochem 83, 184–199. https://doi.org/10.1016/j.soilbio.2015.01.025.
Lavelle, P., Spain, A., Blouin, M., Brown, G., Decaëns, T., Grimaldi, M., Jimenez, J.J., McKey, D., Mathieu, J., Velasquez, E., Zangerlé, A., 2016. Ecosystem engineers in a self-organized soil: a review of concepts and future research questions. Soil Sci 181 (3/4), 91–109. https://doi.org/10.1097/ss.0000000000000155.
Lee, T.C., Kashyap, R.L., Chu, C.N., 1994. Building skeleton models via 3-D medial surface axis thinning algorithms. CVGIP. Graphical Models and Image Processing 56 (6), 462–478. https://doi.org/10.1006/cgip.1994.1042.
Lipkow, E., Betz, O., 2005. Staphylinidae and fungi. Faun. oekol. Mitt 8, 383–411.
Medina-Sauza, R.M., Álvarez-Jiménez, M., Delhal, A., Reverchon, F., Blouin, M., Guerrero-Analco, J.A., Cerdan, C.R., Guevara, R., Villain, L., Barois, I., 2019. Earthworms building up soil microbiota, a review. Front. Environ. Sci. 7, 81. https://doi.org/10.3389/fenvs.2019.00081.
Meurer, K., Barron, J., Chenu, C., Coucheney, E., Fielding, M., Hallett, P., Herrmann, A. M., Keller, T., Koestel, J., Larsbo, M., Lewan, E., Or, D., Parson, D., Parvin, N., Taylor, A., Vereecken, H., Jarvis, N., 2020. A framework for modelling soil structure dynamics induced by biological activity. Glob Change Biol 26 (10), 5382–5403. https://doi.org/10.1111/gcb.15289.
Neithalath, N., Sumanasooriya, M.S., Deo, O., 2010. Characterizing pore volume, sizes, and connectivity in pervious concretes for permeability prediction. Mater Charact 61 (8), 802–813. https://doi.org/10.1016/j.matchar.2010.05.004.
Orth, R.S., Moore, I., Fisher, T.W., Leaner, F.F., 1975. Biological notes on Ocypus olens, a predator of Brown Garden Snail, with descriptions of the larva and pupa (Coleoptera: Staphylinidae). Psyche 82 (3–4), 292–298. https://doi.org/10.1155/1975/36847.
Pierret, A., Capowiez, Y., Belzunces, L., Moran, C.J., 2002. 3D reconstruction and quantification of macropores using X-ray computed tomography and image analysis. Geoderma 106, 247–271. https://doi.org/10.1016/s0016-7061(01)00127-6.
Porre, R.J., van Groenigen, J.W., De Deyn, G.B., de Goede, R.G., Lubbers, I.M., 2016. Exploring the relationship between soil mesofauna, soil structure and N2O emissions. Soil Biol Biochem 96, 55–64. https://doi.org/10.1016/j.soilbio.2016.01.018.
Ruiz, S.A., Or, D., 2018. Biomechanical limits to soil penetration by earthworms: direct measurements of hydroskeletal pressures and peristaltic motions. J R Soc Interface 15 (144), 20180127. https://doi.org/10.1098/rsif.2018.0127.
Schon, N.L., Mackay, A.D., Gray, R.A., Van Koten, C., Dodd, M.B., 2017. Influence of earthworm abundance and diversity on soil structure and the implications for soil services throughout the season. Pedobiologia 62, 41–47. https://doi.org/10.1016/j.pedobi.2017.05.001.
Tharwat, A., 2016. Linear vs. quadratic discriminant analysis classifier: A tutorial. International Journal of Applied. Pattern Recognition 3 (2), 145–180. https://doi.org/10.1504/ijapr.2016.079050.
Xiong, Y., Dai, J., Zhang, X., Huang, G., Furman., A., 2017. Quantitative assessment of the heterogeneity and reproducibility of repacked silica sand columns. Vadose Zone J. 16(13). 10.2136/vzj2017.06.0120.
Wright, J.P., Jones, C.G., 2006. The concept of organisms as ecosystem engineers ten years on: Progress, limitations and challenges. BioScience 56, 203–209. https://doi.org/10.1641/0006-3568(2006)056[0203:tcooae]2.0.co;2.
Zhang, Z., Liu, K., Zhou, H., Lin, H., Li, D., Peng, X., 2018. Three-dimensional characteristics of biopores and non-biopores in the subsoil respond differently to land use and fertilization. Plant soil 428 (1–2), 453–467. https://doi.org/10.1007/s11104-018-3689-3.